Inelastic electron tunneling spectra of MgO-based magnetic tunnel junctions with different electrode designs

Volker Drewello,* Markus Schäfers, Oliver Schebaum, Ayaz Arif Khan, Jana Münchenberger, Jan Schmalhorst, Günter Reiss, and Andy Thomas

Thin Films and Physics of Nanostructures, Bielefeld University, 33615 Bielefeld, Germany

(Received 14 August 2008; published 12 May 2009)

MgO-based magnetic tunnel junctions with up to 230% tunnel magnetoresistance ratio at room temperature and up to 345% at 13 K are prepared. The lower electrode is either exchange-biased or free, while the top electrode is free or an exchanged-biased artificial ferrimagnet, respectively. Additionally, a pseudo-spin-valve (hard-soft switching) design with two unpinned electrodes is used. Inelastic electron-tunneling spectra for each of these systems show a strong variation in the zero-bias anomaly with a reduced peak for some of the junctions. At voltages around 200 mV additional structures are found, which are not known from junctions with lower magneto resistance, such as alumina-based junctions. We discuss the spectra for the different electrode types and compare our findings with respect to barrier material and magnetoresistance ratio.

DOI: 10.1103/PhysRevB.79.174417 PACS number(s): 73.40.Gk, 73.43.Qt, 75.47.−m, 75.70.Cn

I. MOTIVATION

Magnetic tunnel junctions (MTJs) with MgO as a crystalline barrier have been predicted to show very large tunnel magnetoresistance (TMR) ratios.[1,2] Recently, TMR ratios larger than 1000% at low temperature have been shown by Lee *et al.*[3] Nevertheless, the TMR ratio still significantly decreases if higher temperatures or voltages are applied; the room-temperature TMR ratio of the above system is about 500%, limiting the applicability of those systems. One reason for the decreasing TMR values is intrinsic excitations within the junctions which can be studied by inelastic electron-tunneling spetroscopy (IETS).

IETS is a well-established method to characterize nonmagnetic-tunnel junctions[4–6] and was applied to MTJs as well.[7–9] This technique has not only a resolution that is limited only by the intrinsic temperature driven energy broadening of the spectra. The bias-voltage range of the spectra is also only limited by the breakdown voltage of the junctions (typically in the range of a few volts).[10] It is much simpler than laterally resolved methods in terms of sample preparation. Furthermore, it is also closer to applications as it provides information about MTJs that could be used as the base for reconfigurable magnetic logic,[11] magnetic sensors, or magnetic random-access memory.[12]

As indicated by the name, IETS can in principle reveal all inelastic processes in which electrons take part in the tunneling process. An overview can be found in Ref. 13. It is especially possible to excite and identify phonons of the barrier[14] and the electrodes[15] as well as magnons in ferromagnetic materials.[16] Another prominent feature in IET spectra is the zero-bias anomaly. In the dI/dV characteristics a sharp dip at zero bias (up to a few mV) is usually found which results in large peaks in the IET spectrum. In nonmagnetic-tunnel junctions this effect was discovered by Wyatt[17] and has been attributed to single-magnetic impurities.[18,19] A qualitative study of scattering at such impurities, however, has proven to be difficult.[20,21] In MTJs the zero-bias anomaly has always been found since IETS was first applied to MTJs by Moodera *et al.*[7] Recently, also structures at bias voltages higher than 200 mV have been discussed.[22,23] They are of interest because they are presumably connected to the coherent tunneling process which is the base of the high TMR ratios of crystalline MgO barriers.

Here, we measured IET spectra of several tunnel junctions, including MgO-based MTJs and alumina-based systems. We will show differences and similarities of these systems, especially with respect to different electrode types in MgO systems and the different barrier materials. Since the growth of the tunnel barrier is crucial in preparing high TMR MTJs we will describe the layer stacks of the different samples. We will compare our findings to results found in literature and discuss the similarities and specific differences.

II. PREPARATION

The magnetic tunnel junctions are prepared in a magnetron sputter system with a base pressure better than 1×10^{-7} mbar. We used different layer stacks—an overview is given in Table I. The stacks are sputtered on top of a thermally oxidized (50 nm SiO_2) silicon (100) wafer. Stack 1 is a typical system with MgO barrier and Co-Fe-B electrodes. Stack 2 incorporates a pinned artificial ferrimagnet (AFi) as the top electrode. Hard-soft-switching is used to get an antiparallel state in stack 3 (usually called pseudo-spin-valve).

Layer stacks 1—3 are annealed after sputtering for 60 min in a magnetic field of 6500 Oe. This activates the exchange bias and initiates the crystallization of the MgO barrier. Layer stack 1 is annealed at 648 K, stack 2 at 623 K, and stack 3 at 673 K. The different annealing temperatures are chosen to get highest TMR ratios at room temperature (RT) and good magnetic separation in the antiparallel state of the two electrodes at low temperatures. Spectra for the different samples are taken and evaluated. The strength of different inelastic contributions may depend on the annealing temperature. The described approach gives the opportunity to compare the limiting factors for each of the layer stacks. Alternatively, the annealing temperature could haven been identical for all samples. Then the different evolution of in-

TABLE I. The different layer stacks and the corresponding annealing temperatures T_a. Numbers represent the layer thickness in nm. The compositions are Co-Fe-B 40/40/20 at. %, Ni-Fe 81/19 (Permalloy), Co-Fe 70/30, and Mn-Ir 83/17, respectively.

Sample	Lower stack	Barrier	Upper stack	T_a [°C]
1	Ta 10/Ru 30/Ta 5/Ru 5/MnIr 10/CoFeB 2.5	MgO 1.8	CoFeB 2.5/Ta 5/Ru 30/	375
1a	Ta 10/Ru 30/Ta 5/Ru 5/MnIr 10/CoFeB 2.5	MgO 1.8	CoFeB 2.5/Ta 5/Ru 30/	175
2	Ta 5/Ru 40/Ta 5/CoFeB 2.5	MgO 2.1	CoFeB 2.5/Ru 0.88/CoFe 6/MnIr 9/Ru 40/	350
3	Ta 5/Ru 30/Ta 10/Ru 5/CoFeB 4	MgO 2.1	CoFeB 1.5/Ta 5/Ru 30/	400
4	l Cu 30/NiFe 4/MnIr 15/CoFe 3	AlO_x 1.4[a]	NiFe 4/Ta 3/Cu 55/	250[c]
5	Ta 5/Cu 20/Ta 5/Cu 5/Ta 5/MnIr 12/CoFeB 4	AlO_x 1.2[b]	/CoFeB 4/NiFe 3/Ta 5/Cu 20/	275[c]

[a]1.4 nm aluminum+oxidation. See Ref. 24 for details.
[b]1.2 nm aluminum+oxidation.
[c]for 5 min.

elastic contributions could be compared, but one could not be sure if contribution limits the TMR.

Sample 1a is annealed at only 448 K to get a low TMR comparable to alumina-based junctions such as sample 4. The samples are patterned by e-beam lithography and ion-beam etching. The resulting patterns are squares of 25 μm^2. These structures are capped with gold contact pads.

The measurements at 13 K are done in a closed-cycle Helium cryostat (OXFORD Cryodrive 1.5) with a temperature range of 13–330 K by conventional two-probe technique. The bias voltage is always defined with respect to the lower electrode. Thus, negative bias results in electrons tunneling into the upper soft electrode. We use a lock-in technique (STANDFORD SR830 DSP digital two channel Lock-In) with a modulation frequency of 7 kHz and an amplitude of 2 mV (effective, 5.66 mV peak to peak). The resulting measurement is a dI/dV curve which is differentiated numerically to get the d^2I/dV^2 spectra. The thermal smearing of a sharp peak is $5.4k_BT$ [full width at half maximum (FWHM)]. The broadening introduced by the modulation is $1.7\times V_{ac,eff}$ (effective voltage) or $0.6\times V_{ac,p\text{-}p}$ (peak-to-peak value). To see peaks that are limited by the thermal smearing we need $e\times V_{ac,eff}\ll 3.2\times k_BT=0.28\ \text{meV}\times T$ [K]. With our values we have $e\times V_{ac,eff}=2<3$ meV$=5.4k_BT$. For more details see Refs. 6 and 25.

III. RESULTS

A. Bottom pinned Co-Fe-B

Stack 1 is a standard MTJ design with a pinned lower electrode. Our sample exhibits a TMR ratio of over 200% at RT and up to 345% at 13 K. The measured junction has an absolute resistance of 8 kΩ at 13 K. The high resistance of the tunneling barrier ensures that neither line resistances nor inhomogeneous current injection influence the measurement. The absolute resistance of lines and electrodes can be extracted from an MTJ that suffered dielectrical breakdown. It is typically smaller than 50 Ohms. The spectra for parallel- and antiparallel-magnetic states (P state and AP state) are shown in Fig. 1. The zero-bias (ZB) anomaly is clearly visible in both states (peaks are marked ZB in the figure), as well as broader peaks around 85 mV (P) and a smaller peak (in P state) at about 200 mV (C), while at −200 mV a shoulder is visible.

The peaks of the ZB anomaly are located at $(\pm 8\pm 2)$ mV in P state. In the AP state the highest peaks are located at slightly higher bias of (-15 ± 3) mV and $(+19\pm 3)$ mV. This shift to higher energies is commonly observed in other MTJ.[9,22,26] The zero-bias peaks also have shoulders that will be discussed later. The next peaks appear at (-86 ± 5) mV (P) and $(+68\pm 5)$ mV in the P state, thus having a significant asymmetry. In the AP state the peak corresponding to peak P appears at a higher bias voltage of (-100 ± 5) mV. At positive bias no peak is visible. The excitation of MgO phonons at the barrier-electrode interface—which is typical for tunnel junctions[25]—can be identified as the origin of these peaks. The Mg-O-surface phonon has an energy of 80.7 meV (Ref. 27) which corresponds to the peaks we observed. A similar behavior is also found in Refs. 22 and 28

The zero-bias peaks are very symmetric for the P state. In the AP state there is a small asymmetry. More details of these peaks are shown in Fig. 2 for both magnetic states. There, a substructure in the zero-bias peaks is found. In the P state the maxima are at $(\pm 8\pm 1)$ mV (ZB) and shoulders (M) at $(+30\pm 5)$ mV and (-25 ± 5) mV. In the AP state these positions are nearly switched—the maxima are located (M) at

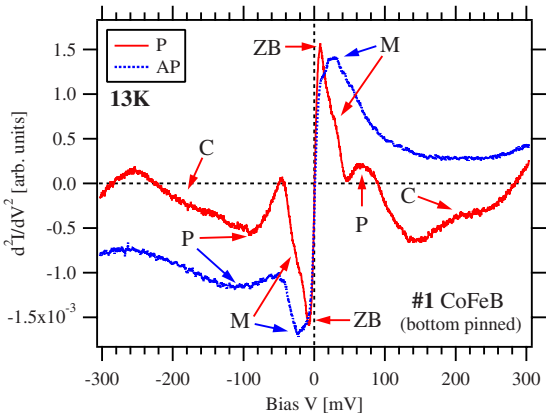

FIG. 1. (Color online) IET spectra of a Co-Fe-B/MgO/Co-Fe-B MTJ (sample 1) in the P state (solid line) and the AP state (dashed line) at 13 K. The ZB and Mg-O phonon peaks (P) are marked. Please note the additional structure (C).

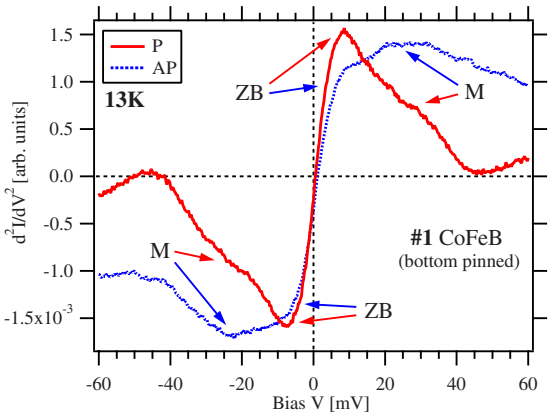

FIG. 2. (Color online) Details of the zero-bias peaks in the P state (solid line) and the AP state (dashed line) at 13 K. Peaks show substructure with maxima (ZB for P state, and *M* for AP state) and shoulders (vice versa).

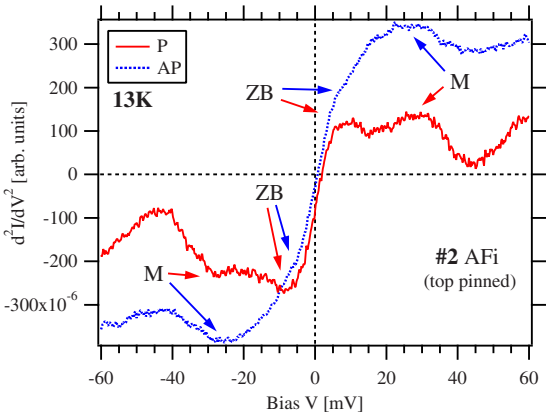

FIG. 4. (Color online) Details of the zero-bias peaks for the AFi sample (stack 2) in the P state (solid line) and the AP state (dashed line) at 13 K. In P state the substructure shows two distinct maxima (ZB and *M*). In AP state there are maxima (*M*) and shoulders (ZB).

$(+27 \pm 5)$ mV and (-24 ± 5) mV while at the other positions (ZB) shoulders appear (more pronounced at negative bias).

B. Top pinned artificial ferrimagnet

In stack 2 a pinned artificial ferrimagnet (AFi) forms the upper electrode, while the lower electrode is the free one. The measured junction shows an absolute resistance of 23 kΩ at 13 K. The spectra in both magnetic states shown in Fig. 3 look significantly different to those of stack 1. First of all the peak heights are much smaller in P state compared to AP state. In both states the peaks of the ZB anomaly (ZB) are much smaller as in the sample 1 [relative to the corresponding phonon peaks (*P*) in the same state].

Details of the zero-bias peaks are shown in Fig. 4. In P state the substructure is visible in form of two peaks with clearly separated maxima. The first peaks (ZB) are at $(\pm 8 \pm 1)$ mV and the other at $(\pm 28 \pm 3)$ mV (*M*). In the AP state the maxima are at $(\pm 26 \pm 5)$ mV (*M*) as it was the case in sample 1. At the other position (ZB) at around ± 8 mV shoulders can be recognized.

C. Co-Fe-B pseudo-spin-valve

Sample 3 is a pseudo-spin-valve, i.e., the AP state is possible due to different switching fields of the upper and lower electrode. The investigated MTJ showed an absolute resistance of 4.2 kΩ. The spectra are shown in Fig. 5. They look like an intermediate piece between samples 1 and 2. In the P state the peaks (ZB) (at -6 ± 1 and $+8 \pm 1$ mV) are smaller than in sample 1 which makes the shoulders (*M*) very pronounced. The phonon peaks (*P*) at $(\pm 71 \pm 2)$ mV and the structures *C* around 200 mV are very similar to those in sample 2. Moreover, everything except the innermost peaks looks nearly identical to sample 2. In comparison to sample 1 (Fig. 1) structure *C* is very different. In the AP state the spectrum looks very much like that of sample 2. Only the relative height of the ZB peaks is a bit larger. Also, the struc-

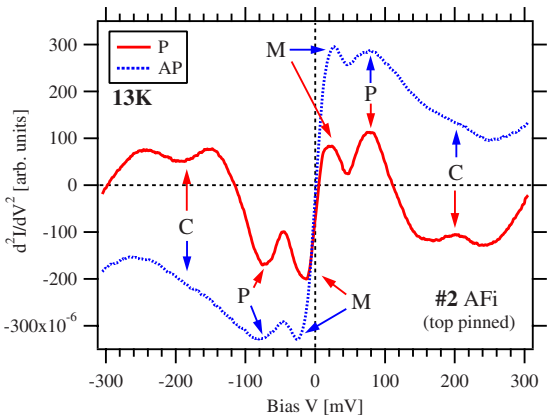

FIG. 3. (Color online) IET spectra of sample 2 (AFi as pinned electrode) in the P state (solid line) and the AP state (dashed line) at 13 K. The same peaks as in sample 1 are found: the ZB, magnon (*M*), and Mg-O phonon peaks (*P*) are marked. An additional feature (*C*) is found for both magnetic states and polarities.

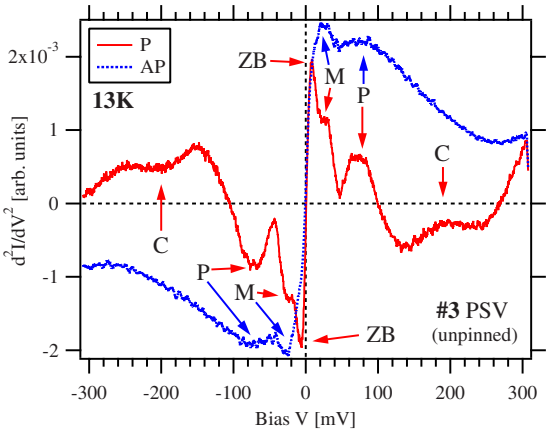

FIG. 5. (Color online) IET spectra of sample 3 (hard-soft switching) in the P state (solid line) and the AP state (dashed line) at 13 K. The same peaks as in samples 1 and 2 are found: ZB, magnon (*M*), and Mg-O phonon peaks (*P*) are marked. The additional peaks are found in P state (*C*).

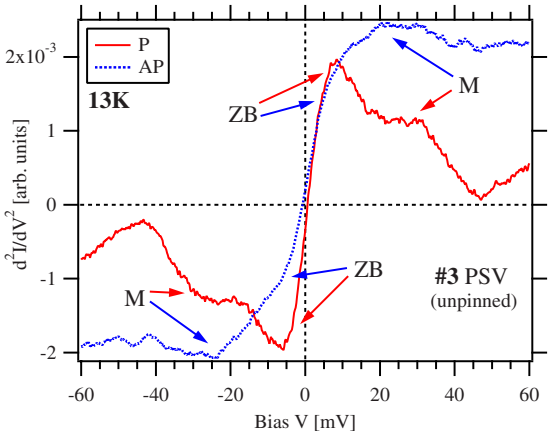

FIG. 6. (Color online) Details of the zero-bias peaks for the pseudo-spin-valve sample (stack 3) in the P state (solid line) and the AP state (dashed line) at 13 K. In P state the substructure shows a distinct maximum (ZB) and very pronounced shoulders (*M*). This behavior fits in between samples 1 and 2. In AP state there are maxima (*M*) and shoulders (ZB).

tures at 200 mV (*C*) are not distinguishable in AP state.

A closer look at the lower bias region (Fig. 6) reveals that only the first peaks in P state (ZB) are strongly different compared to sample 2. The AP spectrum is very similar to the one of sample 2.

IV. DISCUSSION

In Table II the different features of the spectra of all samples are summarized. We will now discuss the different aspects of our measurements.

A. Low bias peaks in the spectra of MgO based samples

When comparing the spectra of the MgO-based samples, in which the electrode design was varied (1–3), we find the largest difference in the distinct peaks at low-bias voltage. In the P state the peaks in sample 1 have very distinct maxima (ZB, Fig. 2) which show small shoulders (*M*). These shoulders can be overlooked if insufficient resolution or zoom is used. In sample 2 (Fig. 4) the initial peaks are much smaller and distinct peaks at the position of the former shoulders can be identified. These spectra are very comparable to those presented by Matsumoto *et al.*[29] Sample 3 (Fig. 6) shows an intermediate state, where the first peaks are not as high as in sample 1 and the shoulders are very clearly seen. For the different samples the peaks (or shoulders) are located at the same positions within small range of error. They only vary in their relative intensity and width. Therefore the intrinsic excitation processes responsible for these structures are supposedly the same for the different samples. The first peak (ZB) is comparable in height for the P and the AP state in each sample, which means the underlying excitation is not depending on the magnetic configuration or external field. This is different for the shoulders or second peaks (*M*). The underlying excitation seems much more prominent in the AP spectra, where these "shoulders" indeed form the maxima in the spectra. Thus, what might look like a shift in the position of the peak could be a change in the relative height of two different peaks. This is most clearly seen in sample 2 (Fig. 3). The maximum seems just "shifting" if going from the P to the AP state but in the higher resolved spectra (Fig. 4) the peaks and shoulders can be separated.

The very first peak is the zero-bias anomaly caused by magnetic impurities. There is no dependence on the magnetic state of the junction. The peaks are most pronounced in sample 1, presumably because of diffusion of Manganese from the antiferromagnet.[30,31] The zero-bias peak in sample 2 is smaller than in sample 1 because of the additional layers of Ruthenium and Co-Fe between the antiferromagnet and the barrier, which partially prevents the diffusion of manganese.[31] In sample 3 no Mn is present, so the ZB peaks are also smaller than in sample 1. They are not as small as in

TABLE II. An overview of our findings for the different samples. The visibility of the listed features is evaluated [++ strong, + distinct, ∘ fair (e.g., shoulder), and − not visible]. The upper half shows the parallel magnetic state, the lower half shows the antiparallel magnetic state. Please note that the order of samples has been changed in order to emphasize similarities and differences, respectively. We find that sample 2 is the most feature rich, especially in the AP state. Samples 3, 1, and 5 show sequentially less distinct features, but at the same time larger (and broader) low-bias peaks. We also find that the MgO-based samples look similar, with the exception of sample 1a. This sample—annealed at lower temperature—is more similar to the alumina-based sample 4.

Feature				MgO			Alumina		MgO
State	Peak	Bias [mV]	Suggested origin	2	3	1	5	4	1a
P	*C*	190–230	"high TMR feature"	++	++	+	+	−	−
	P	≈81/120	barrier phonons	++	++	++	∘	+	∘
	M	20–35	interface magnons	++	+	∘	∘	−	−
	ZB	≤15	zero bias/impurities	∘	+	++	+	+	+
AP	ZB	≤15	zero bias/impurities	∘	∘	∘	∘	∘	+
	M	20–35	interface magnons	+	+	+	+	+	−
	P	≈81/120	barrier phonons	+	−	∘	∘	+	−
	C	190–230	"high TMR feature"	∘	−	−	−	−	−
	TMR ratio at room temperature [%]			210	220	210	72	50	38

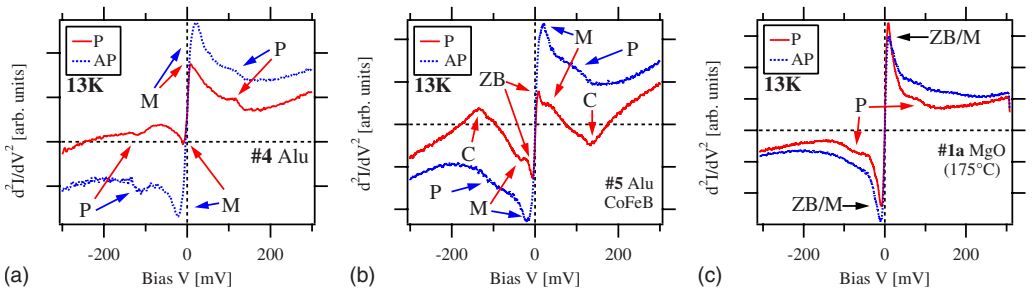

FIG. 7. (Color online) IET spectra of sample 4 (a), 5 (b), and 1a (c) in the P state (solid line) and the AP state (dashed line) at 13 K. Basically, the same peaks are found: the ZB, magnon (M), and phonon peaks (P) are marked, the latter are less pronounced in the spectra of sample 1a. At higher voltage no structure is found for samples 1a and 4, but for sample 5 large dips can be found around 130 mV (C) in parallel state, which also reduce peaks M to smaller shoulders.

sample 2—other impurities may contribute at higher annealing temperatures.

More impurities should lower the TMR ratio of a junction, which is the case for our samples at room temperature. We always observe higher zero-bias peaks with lower TMR ratios which supports our interpretation. The TMR ratios of sample 1 and sample 2 are as high as 210%. However, if sample 2 is annealed at higher temperature of 400 °C a TMR ratio of over 230% is achieved. We can conclude that for sample 2 the TMR ratio is not limited by diffusion but subtotal recrystallization.[32] The pseudo-spin-valve (sample 3) shows up to 220% depending on the magnetic separation in an individual junction, which fits with its intermediate position in the strength of the zero-bias peak.

The second peak (or shoulder) (M in Figs. 2, 4, and 6) strongly depends on the magnetic state: it is roughly twice as high in the AP state compared to the P state. This is a major difference compared to the zero-bias peak. We suggest that this peak corresponds to the maximum probability for magnon excitation at the ferromagnet-insulator interfaces, which is proposed to be higher in the AP state.[29,33] Also, possible magnon excitations have been identified at similar bias voltage by other groups.[29,34]

B. Spectra of MgO and alumina based junctions—Can we see coherence?

We also investigated alumina-based MTJs in order to compare the results to our MgO-based systems. Alumina-based junctions have an amorphous barrier and only incoherent tunneling takes place. Sample 4 has Co-Fe and Ni-Fe electrodes and a TMR ratio of 50% and 70% at room temperature and 13 K, respectively. The spectra are shown in Fig. 7(a). Sample 5 has two Co-Fe-B electrodes and shows a TMR ratio of 72% and 110% at room temperature and 13 K, respectively. The corresponding spectra can be found in Fig. 7(b).

The first thing to be noticed in the spectra is the small zero-bias anomaly in these two samples. The zero-bias anomaly is previously explained by the diffusion of magnetic impurities. Therefore, the small peaks can be explained by the low annealing temperature and the short annealing time of only a few minutes. The large maximum in the AP state is mainly caused by the second peak, identified as excitation of interface magnons before. The spectra also show peaks around 120 mV. These were identified as Al-O phonon peaks before.[25] For sample 4 there is no further structure at higher bias voltage.

We prepared an MgO-based sample [1a] identical to sample 1 but was annealed at only 175 °C for 1 h. At this temperature the recrystallization of Co-Fe-B is not established[35] and therefore no coherence is possible. This preparation process makes it comparable to alumina-based sample 4. It shows TMR ratios of 38% and 61% at room temperature and 13 K. The spectra presented in Fig. 7(c) show magnon and phonon peaks but no further structure. The first peaks are higher for the MgO sample, but they are not sharp enough to distinguish between what we called zero bias and magnon excitation before. Nevertheless, the spectra are very similar to those of sample 4 (also compare, e.g., Ref. 9). Especially, there is no structure beyond the phonon peak at 81 or 120 mV, respectively.

This is different for the spectra of the MgO-based samples 1 to 3. For these samples additional structures around 200 mV are clearly seen in P state (Figs. 1, 3, and 5). In this bias region, peaks are embedded in wide dips (IETS signal <0) for all samples. In the work of Ono *et al.*[28] similar structures in their IET spectra are visible at 250 mV and are also embedded in a strong dip. It should be noted that only the wide dip is found in most other publications[23,28,29] at bias voltages of 250–400 mV. The small peak within is not always visible, while in this work it is always found in the P state and for sample 2 also in the AP state.

This structure is discussed as evidence for coherent tunneling through MgO.[22,23,28] However, we cannot conclude that the dip structure found in the MgO-based MTJs with high TMR ratio is caused by coherent tunneling. The spectra of the alumina-based sample 5 also show deep dips in the P state [Fig. 7(c)]. The d^2I/dV^2 signal becomes negative as it is the case for the MgO-based junctions. However, these dips are located at lower voltages of around 130 mV. This also leads to a reduction in the phonon peaks in the P state.

If all measurements are compared an interesting tendency can be found—the dip gets more pronounced with a higher TMR ratio of the junction. However, no samples were available with TMR ratios between the 72% of sample 5 and 200%. We suggest that a highly spin-polarized electrode material without a crystalline barrier should be investigated to get higher TMR ratios while maintaining incoherent tunnel-

ing. A possible candidate would be a Heusler compound electrode and an alumina barrier. It would be possible to judge whether the dip structure is related to the barrier material, a high TMR ratio, or even coherent tunneling, if, e.g., junctions with TMR ratios around 150% and alumina as well as MgO barriers could be prepared.

V. SUMMARY

In summary, we prepared MgO-based magnetic tunnel junctions which show up to 230% TMR at room temperature and 345% TMR at 13 K. We measured IET spectra of those systems in parallel and antiparallel magnetic state. Several ferromagnetic electrode designs were used in order to clarify the origin of the peaks. The zero-bias anomaly could be identified, which is caused by magnetic impurities. A second peak was found, which strongly differs for parallel and antiparallel magnetic state. This is attributed to the excitation of magnons.

A pronounced additional structure at 200 mV is found in parallel state which is stronger the higher the TMR. This cannot be attributed to coherent tunneling (or the MgO barrier) as it is also found in alumina-based junctions.

ACKNOWLEDGMENTS

We gratefully acknowledge Catherine A. Jenkins for helpful discussions and the DFG (Grant No. RE 1052/13-1) for financial support.

*drewello@physik.uni-bielefeld.de

[1] W. H. Butler, X.-G. Zhang, T. C. Schulthess, and J. M. MacLaren, Phys. Rev. B **63**, 054416 (2001).
[2] J. Mathon and A. Umerski, Phys. Rev. B **63**, 220403(R) (2001).
[3] Y. M. Lee, J. Hayakawa, S. Ikeda, F. Matsukura, and H. Ohno, Appl. Phys. Lett. **90**, 212507 (2007).
[4] R. C. Jaklevic and J. Lambe, Phys. Rev. Lett. **17**, 1139 (1966).
[5] A. Geiger, B. Chandras, and J. Adler, Phys. Rev. **188**, 1130 (1969).
[6] J. Klein, A. Léger, M. Belin, D. Défourneau, and M. J. L. Sangster,Phys. Rev. B **7**, 2336 (1973).
[7] J. S. Moodera, J. Nowak, and R. J. M. van de Veerdonk, Phys. Rev. Lett. **80**, 2941 (1998).
[8] R. J. M. van de Veerdonk, J. S. Moodera, and W. J. M. de Jonge, J. Magn. Magn. Mater. **198-199**, 152 (1999).
[9] X.-F. Han, A. C. C. Yu, M. Oogane, J. Murai, T. Daibou, and T. Miyazaki, Phys. Rev. B **63**, 224404 (2001).
[10] A. A. Khan, J. Schmalhorst, A. Thomas, O. Schebaum, and G. Reiss, J. Appl. Phys. **103**, 123705 (2008).
[11] A. Thomas, D. Meyners, D. Ebke, N.-N. Liu, M. D. Sacher, J. Schmalhorst, G. Reiss, H. Ebert, and A. Hütten, Appl. Phys. Lett. **89**, 012502 (2006).
[12] S. A. Wolf, D. D. Awschalom, R. A. Buhrman, J. M. Daughton, S. von Molnar, M. L. Roukes, A. Y. Chtchelkanova, and D. M. Treger, Science **294**, 1488 (2001).
[13] C. J. Adkins and W. A. Phillips, J. Phys. C **18**, 1313 (1985).
[14] J. G. Adler, Solid State Commun. **7**, 1635 (1969).
[15] T. T. Chen and J. G. Adler, Solid State Commun. **8**, 1965 (1970).
[16] D. C. Tsui, R. E. Dietz, and L. R. Walker, Phys. Rev. Lett. **27**, 1729 (1971).
[17] A. F. G. Wyatt, Phys. Rev. Lett. **13**, 401 (1964).
[18] J. A. Appelbaum, Phys. Rev. **154**, 633 (1967).
[19] J. A. Appelbaum and L. Y. L. Shen, Phys. Rev. B **5**, 544 (1972).
[20] R. H. Wallis and A. F. G. Wyatt, J. Phys. C **7**, 1293 (1974).
[21] S. Bermon, D. E. Paraskevopoulos, and P. M. Tedrow, Phys. Rev. B **17**, 2110 (1978).
[22] G.-X. Miao, K. B. Chetry, A. Gupta, W. H. Butler, K. Tsunekawa, D. Djayaprawira, and G. Xiao, J. Appl. Phys. **99**, 08T305 (2006).
[23] M. Mizuguchi, *et al.*, J. Appl. Phys. **99**, 08T309 (2006).
[24] J. Schmalhorst and G. Reiss, Phys. Rev. B **68**, 224437 (2003).
[25] E. Wolf, in *Principles of Electron Tunneling Spectroskopy*, International Series of Monographs on Physics No. 71 edited by R. Elliot, J. Krumhansl, W. Marshall, and D. Wilkinson (Oxford University Press, New York, 1989).
[26] J. Murai, Y. Ando, M. Kamijo, H. Kubota, and T. Miyazaki, Jpn. J. Appl. Phys., Part 2 **38**, L1106 (1999).
[27] P. A. Thiry, M. Liehr, J. J. Pireaux, and R. Caudano, Phys. Rev. B **29**, 4824 (1984).
[28] K. Ono, T. Daibou, S.-J. Ahn, Y. Sakuraba, T. Miyakoshi, T. Morita, Y. Kikuchi, M. Oogane, Y. Ando, and T. Miyazaki, J. Appl. Phys. **99**, 08A905 (2006).
[29] R. Matsumoto, *et al.*, Solid State Commun. **136**, 611 (2005).
[30] P. V. Paluskar, C. H. Kant, J. T. Kohlhepp, A. T. Filip, H. J. M. Swagten, B. Koopmans, and W. J. M. de Jonge, J. Appl. Phys. **97**, 10C925 (2005).
[31] J. Hayakawa, S. Ikeda, Y. M. Lee, F. Matsukura, and H. Ohno, Appl. Phys. Lett. **89**, 232510 (2006).
[32] At low temperatures the sample with over 230% at RT-TMR ratio showed no sufficient magnetic separation for TMR measurements or IETS of a defined magnetic state.
[33] V. Drewello, J. Schmalhorst, A. Thomas, and G. Reiss, Phys. Rev. B **77**, 014440 (2008).
[34] P. V. Paluskar, F. L. Bloom, J. T. Kohlhepp, H. J. M. Swagten, B. Koopmans, and E. Snoeck, Appl. Phys. Lett. **91**, 222501 (2007).
[35] M. Jimbo, K. Komiyama, Y. Shirota, Y. Fujiwara, S. Tsunashima, and M. Matsuura, J. Magn. Magn. Mater. **165**, 308 (1997).